

Subscriber access provided by UNIV OF WISCONSIN - MADISON

Biological and Environmental Phenomena at the Interface

Peripheral Membrane Proteins Facilitate Nanoparticle Binding at Lipid Bilayer Interfaces

Eric S Melby, Caley Allen, Isabel Foreman-Ortiz, Emily Caudill, Thomas R. Kuech, Ariane M. Vartanian, Xi Zhang, Catherine J. Murphy, Rigoberto Hernandez, and Joel A. Pedersen

Langmuir, Just Accepted Manuscript • Publication Date (Web): 13 Aug 2018

Downloaded from http://pubs.acs.org on August 13, 2018

Just Accepted

"Just Accepted" manuscripts have been peer-reviewed and accepted for publication. They are posted online prior to technical editing, formatting for publication and author proofing. The American Chemical Society provides "Just Accepted" as a service to the research community to expedite the dissemination of scientific material as soon as possible after acceptance. "Just Accepted" manuscripts appear in full in PDF format accompanied by an HTML abstract. "Just Accepted" manuscripts have been fully peer reviewed, but should not be considered the official version of record. They are citable by the Digital Object Identifier (DOI®). "Just Accepted" is an optional service offered to authors. Therefore, the "Just Accepted" Web site may not include all articles that will be published in the journal. After a manuscript is technically edited and formatted, it will be removed from the "Just Accepted" Web site and published as an ASAP article. Note that technical editing may introduce minor changes to the manuscript text and/or graphics which could affect content, and all legal disclaimers and ethical guidelines that apply to the journal pertain. ACS cannot be held responsible for errors or consequences arising from the use of information contained in these "Just Accepted" manuscripts.



Peripheral Membrane Proteins Facilitate Nanoparticle Binding at Lipid Bilayer Interfaces

Eric S. Melby, †,‡,a,b Caley Allen, $^{\$,a,c}$ Isabel U. Foreman-Ortiz, Emily R. Caudill, Thomas R.

Kuech, Ariane M. Vartanian, A Xi Zhang, Catherine J. Murphy, Rigoberto Hernandez,**,8,*

Joel A. Pedersen*,†,|

Department of Chemistry, University of Illinois at Urbana – Champaign, 600 S. Mathews Ave., Urbana, IL 61801

* Corresponding Authors:

Joel A. Pedersen; University of Wisconsin, 1525 Observatory Drive, Madison, WI, 53706; 608-263-4971; joelpedersen@wisc.edu

Rigoberto Hernandez; Department of Chemistry, Johns Hopkins University, Baltimore, MD 21218, 410-516-4018; r.hernandez@jhu.edu

KEYWORDS: supported lipid bilayer, quartz crystal microbalance with dissipation monitoring, peripheral membrane protein, nanoparticles, nanoplasmonic sensing, nano-bio interface, molecular dynamics

[†] Environmental Chemistry and Technology Program, University of Wisconsin – Madison, 1525 Observatory Dr., Madison, WI 53706

[‡] Environmental and Molecular Sciences Laboratory, Pacific Northwest National Laboratory, 3335 Innovation Blvd., Richland, WA 99354

[§] Department of Chemistry, Johns Hopkins University, Baltimore, MD 21218;

Department of Chemistry, University of Wisconsin – Madison, 1101 University Ave., Madison, WI 53706

^a These authors contributed equally to the work.

^b Present address: Chemistry Department, Columbia Basin College, 2600 N. 20th Ave., Pasco, WA 99301

^c Present address: EBICS: Emergent Behavior of Integrated Cellular Systems, Massachusetts Institute of Technology, NE47-321, Cambridge, Massachusetts 02139

^d Present address: Nature Communications, 1 New York Plaza, 1 FDR Dr., New York, NY 10004

ABSTRACT: Molecular understanding of the impact of nanomaterials on cell membranes is critical for the prediction of effects that span environmental exposures to nano-enabled therapies. Experimental and computational studies employing phospholipid bilayers as model systems for membranes have yielded important insights but lack the biomolecular complexity of actual membranes. Here, we increase model membrane complexity by incorporating the peripheral membrane protein cytochrome c and studying the interactions of the resulting membrane systems with two types of anionic nanoparticles. Experimental and computational studies reveal that the extent of cytochrome c binding to supported lipid bilayers depends on anionic phospholipid number density and headgroup chemistry. Gold nanoparticles functionalized with short, anionic ligands or wrapped with an anionic polymer do not interact with silica-supported bilayers composed solely of phospholipids. Strikingly, when cytochrome c was bound to these bilayers, nanoparticles functionalized with short anionic ligands attached to model biomembranes in amounts proportional to the number of bound cytochrome c molecules. In contrast, anionic polymer-wrapped gold nanoparticles appeared to remove cytochrome c from supported lipid bilayers in a manner inversely proportional to the strength of cytochrome c binding to the bilayer; this reflects the removal of a weakly bound pool of cytochrome c as suggested by molecular dynamics simulations. These results highlight the importance of the surface chemistry of both the nanoparticle and the membrane in predicting nano-bio interactions.

INTRODUCTION

Engineered colloidal nanomaterials are being deployed as diagnostic, imaging, delivery, and therapeutic agents. Predictive success requires a mechanistic understanding of the interaction of nanomaterials with cell or organelle membranes. Such knowledge is also needed to assess

potential environmental health and safety risks associated with use of engineered nanomaterials.¹ The cytoplasmic membrane represents the initial point of contact between a nanoparticle and eukaryotic cells.² After internalization, nanoparticles may interact with a variety of intracellular membranes. Interactions of nanoparticles with cell membranes may alter lipid ordering,³ lead to attachment⁴ and cell entry via passive diffusion or endocytosis,^{5,6} induce membrane permeabilization,^{7,8} or cause lipid extraction.^{9,10} Mechanistic understanding of nanoparticle interactions at biological interfaces requires consideration of the chemical and physical properties of both the nanoparticle and the cellular membrane. In eukaryotes, cell membranes are composed of a mixture of glycerophospholipids, sphingolipids, sterols,¹¹ and contain an abundance of integral, peripheral, and lipid-anchored proteins, some of which are glycosylated.¹²

The biomolecular complexity of cellular membranes poses a challenge to developing a mechanistic understanding of their interactions with nanomaterials. Phospholipid bilayers have been employed as chemically and physically tunable cell membrane mimics to study nanoparticle interactions with cell surfaces. The majority of these studies use single-phase supported lipid bilayers composed of a single or binary mixtures of phospholipids. ^{3,8,13–22} Both experimental and computational studies have provided valuable insights into the influence of phospholipid properties in nanoparticle interactions with cell membranes, including nanoparticle-induced membrane hole formation ^{8,22} and nanoparticle penetration of lipid bilayers. ^{13,14} They have revealed the importance of electrostatics in governing nanoparticle-membrane interactions. ^{15,21} We previously demonstrated that, relative to bilayers composed of a single phospholipid species, the presence of liquid-ordered domains ²³ or glycans ²⁴ can strongly influence nanoparticle interaction with model biomembranes.

Membrane-associated proteins can comprise more than 50% of cellular membrane mass in eukaryotes and bacteria¹² and represent >20% of the total proteome across all three domains of life.^{25,26} Much research has been directed toward understanding the interaction of soluble proteins with nanoparticle surfaces and the formation of biomolecular coronas.^{27–30} In contrast, and despite their prevalence and importance in cell membranes, membrane proteins have received little study in the context of their interaction with nanoparticles.^{31–33} Recent reviews of model membrane studies reveal a dearth of investigations incorporating proteins.^{18,34–36} A few studies investigating nanoparticle interaction with lung surfactant have included surfactant-associated proteins.^{37,38} Gold nanoparticle interaction with glucose-6-phosphatase in phospholipid monolayers has been examined.³⁹ Because this transmembrane protein contains nine transmembrane helices and therefore spans the bilayer membrane, the orientation of glucose-6-phosphatase in a monolayer at the air-water interface likely does not correspond to that *in vivo*.

The primary objective of this study is to investigate the influence of a model peripheral membrane protein on anionic nanoparticle interaction with model biomembranes. To accomplish this objective, we examined the influence of the peripheral membrane protein cytochrome c (cyt c; Figure 1) on nanoparticle interaction with model supported bilayers composed of zwitterionic 1,2-dioleoyl-sn-glycero-3-phosphocholine (18:1 phosphatidylcholine, DOPC) alone or in combination with anionic 1',3'-bis[1,2-dioleoyl-sn-glycero-3-phospho]-sn-glycerol (18:1 cardiolipin, TOCL) or anionic bovine liver α -phosphatidylinositol (Liver PI, a mixture of phosphatidylinositol lipids varying in acyl chain length, degree of saturation, and position of double bonds) (Figure S1). We focused on the highly conserved peripheral membrane protein cyt c because of the wealth of literature that exists on its interaction with lipid bilayers.

Cytochrome c associates with the inner mitochondrial membrane, is an important component of the electron transport chain, and plays a role in apoptosis when released into the cytosol. We conducted molecular dynamics (MD) simulations to investigate the orientation and conformation of cyt c on bilayers representative of those used in this study. We investigated the interaction of cyt c-containing model membrane systems with nanoparticles functionalized with small anionic ligands and wrapped in anionic polymers.

RESULTS AND DISCUSSION

Formation of Supported Lipid Bilayers Incorporating Cytochrome c. We employed simultaneous quartz crystal microbalance with dissipation monitoring (QCM-D) and nanoplasmonic sensing (NPS) to monitor supported lipid bilayer formation^{44,45} and subsequent association of the peripheral membrane protein cyt c with them. The acoustic mass calculated from QCM-D frequency data includes the mass of the analyte and dynamically coupled solvent and can therefore be considered a "wet" mass. The optical mass derived from NPS measurements does not include a contribution from the solvent because the refractive index of the solution is taken as the reference and can be considered a "dry" mass. Simultaneous measurement of acoustic and optical mass by combined QCM-D and NPS allows estimation of adlayer water content.

We formed supported lipid bilayers composed of DOPC alone and in combination with TOCL or LPI using the vesicle fusion method (Figure S2)⁴⁴ and then incorporated cyt c into the bilayers containing anionic phospholipids. (Cytochrome c did not attach to pure DOPC bilayers.) Figure 2A shows example results from a combined QCM-D/NPS experiment for the attachment of cyt c to a supported DOPC bilayer incorporating 17.6 mol% TOCL (phospholipid compositions of all bilayers are given in mol%). The cyt c adlayer was rigidly coupled to the

oscillations of the sensor crystal allowing use of the Sauerbrey equation 46,47 (equation 1, *vide infra*) to estimate acoustic surface mass density. Simultaneous monitoring of $\Delta\lambda_{\rm max}$ via NPS allowed the optical surface mass density of cyt c to be calculated. The large difference between the acoustic and optical surface mass densities reflects the substantial mass of water associated with the cyt c adlayer as sensed by QCM-D. The acoustic and optical surface mass densities for cyt c adlayers for all bilayer systems investigated are reported in Table S2.

The mass of cyt c binding to supported lipid bilayers increased with the amount of negative charge imparted by incorporation of anionic phospholipids (p < 0.001; Figure 2B), consistent with expectations based on electrostatic interactions.⁴⁸ Incorporation of increasing amounts of anionic phospholipids (TOCL or Liver PI) into DOPC vesicles resulted in increasingly negative zeta potentials (ζ) as determined by laser Doppler microelectrophoresis (Table S3). We therefore infer that the ζ of the supported lipid bilayers similarly decreased with increasing incorporation of anionic phospholipids. We note that the phosphatidylinositol head groups of the Liver PI molecules carry a single negative charge, while those of TOCL bear two negative charges. Cytochrome c is expected to exhibit an approximate +8 charge at pH 7.4 (Figure 1).⁴⁹

To assess the strength of cyt c association with model membranes varying in phospholipid composition, we examined the effect of incremental increases in NaCl concentration (from 0.01 M to 0.1 M) on cyt c dissociation from supported lipid bilayers. The slope of the linear portion of the dissociation curves decreased with increasing anionic phospholipid content in the bilayer (Figure 2C). These results are consistent with reduction in the electrostatic attraction of cyt c to the bilayers containing anionic lipids due to charge screening, leading to cyt c dissociation, and demonstrate that the strength of cyt c binding to supported lipid bilayers correlates directly with the amount of negative charge within the bilayer. We observed that cyt c bound to bare

silica showed the smallest amount of dissociation with increasing NaCl concentration, likely due to this surface carrying a strong negative ζ at pH 7.4 (approximately -110 mV).⁵² In the case of cyt c bound to either 17.6% TOCL bilayers and to silica, complete dissociation of cyt c did not occur even upon increasing the NaCl concentration to 0.1 M. For these systems, we further raised the final the NaCl concentration to 0.15 M, and following this increase, $8.2 \pm 2.0\%$ of cyt c originally bound to the 17.6% TOCL supported lipid bilayer remained (32 \pm 8.2 ng·cm⁻²), whereas $48.4 \pm 8.8\%$ remained on the silica surface (140 \pm 24 ng·cm⁻²). The highest concentration of TOCL employed (17.6%) falls within the range expected in the inner mitochondrial membrane of both mammals and yeast; $^{11} \sim 10\%$ cyt c remains bound to the inner mitochondrial membrane at physiological ionic strength. 53

Cytochrome *c* **Structure and Orientation on Bilayers Containing Anionic Phospholipids.** We next sought to determine which surface(s) of cyt *c* face the phospholipid bilayer and which face the solution (and are therefore more likely to interact with the nanoparticles we studied). Despite being perhaps the most thoroughly investigated peripheral membrane protein, the location of the phospholipid binding site(s) and the bilayer-anchoring mechanism for cyt *c* has not been fully resolved. In the absence of crystal structures of cyt *c* bound to TOCL, the precise site(s) of binding to or preferred binding orientation(s) on TOCL can be assessed via atomistic molecular dynamics (MD) simulations. Sites A, C, L, N (Figure 1), and several lysine residues have been implicated as possible binding sites to anionic phospholipids. 40,41,51,54–58 We therefore focused on observables that characterize their relative positions in MD simulations. All MD simulations included explicit water and counter ions.

Combinatoric Panel of Cytochrome c and Bilayer Simulations. Nine trajectories were integrated using molecular dynamics on starting configurations while varying the membrane

composition and the cyt c orientation. The three lipid bilayers investigated were composed of 100% DOPC, a 9:1 mixture of DOPC and cardiolipin (DOPC:TOCL), or a 9:1 mixture of DOPC and SAPI (DOPC: SAPI) (Figure S1). (The 18:0-20:4-phosphoinositol lipid SAPI is the second most abundant species in the Liver PI mixture used in the experiments and serves to illustrate the effect of Liver PIs on cyt c binding.) For each of these, we conducted simulations with cyt c initially aligned in one of three possible starting orientations – denoted by face 1, face 2, and face 3 – relative to the surface of the lipid bilayers (Figure 3). Each protein-bilayer system was propagated for 200 ns. To characterize the preferential orientation and overall structural conformations of cyt c across the different simulations, we monitored the following observables: (i) the distances between the average position of the phosphorus atoms in the upper membrane leaflet and the center of mass (COM) of each of the three selected faces (1, 2, and 3) of cyt c and the COM of the entire protein (Figure 1); (ii) the number of hydrogen-bonding interactions between each face of cyt c and selected groups in the lipids, including glycerol, phosphate, and choline groups (Figure S4); (iii) the distances between the specific amino acids in the anionic phospholipid binding sites of cyt c (L, C, A, N, and the three lysine residues involved in cardiolipin recognition) and the surface of the upper leaflet (Figures S5-S8); and (iv) the secondary and tertiary structural dynamics and conformational fluctuations of cyt c along each 200 ns MD trajectory (Figures S9-S12).

Effects of Bilayer Composition and the Initial Orientation of Cytochrome c on Binding by Simulation. We monitored the average positions (COMs) of the amino acids that comprise each cyt c face (1, 2, and 3), in addition to the COM of the entire protein, relative to the membrane plane across all nine trajectories (Figure 4). A value of 0 Å would occur if the COM of the selected residues were located on the plane at the average position of the phosphorus atoms in

the upper leaflet of the model membrane. Regardless of the starting orientation (face 1, 2, or 3), when cyt c is positioned atop the zwitterionic bilayer (Figure 4A-C), the protein dissociated away from the bilayer and became completely solvated.

When the anionic phospholipids SAPI (Figure 4D-F) or TOCL (Figure 4G-I) were incorporated into the bilayer, cyt c physisorbed to the model membrane surface in one of two final orientations. For each starting orientation of cyt c on the DOPC:SAPI bilayer, the final orientation of the protein was such that faces 1 and 2 were in closest proximity to the bilayer surface. This is consistent with the experimental result of no observed cyt c interaction with bilayers composed solely of DOPC. For DOPC:SAPI with cyt c face 1 or face 2 oriented toward the bilayer, the alignment of protein with respect to the bilayer surface remained fairly constant throughout the entire trajectory. However, when face 3 was initially positioned closest to the DOPC:SAPI surface, this face rotated away from the DOPC:SAPI surface. In its final orientation, a mixture of amino acids from faces 1 and 2 were closest to the DOPC:SAPI membrane.

When TOCL was introduced into the bilayer, the dynamics and observed orientations of cyt *c* became more complex. As with the DOPC:SAPI bilayer, when face 3 was initially aligned toward the DOPC:TOCL surface, this face rotated away from the bilayer, resulting in faces 1 and 2 pointing towards the DOPC:TOCL surface. However, when the protein was initially oriented such that face 1 was closest to the DOPC:TOCL bilayer, a different protein alignment was observed. Unlike in the final configurations of the trajectories stemming from the other initial orientations on DOPC:SAPI, in which the amino acids from faces 1 and 2 were closest to the bilayer surface, here faces 1 and 2 rotated away from the DOPC:TOCL surface, resulting in faces 1 and 3 having the closest proximity.

The trends seen in the COM distances of Figure 4 were further supported by the hydrogen bonding contacts between each face of the protein and bilayer surface observed along each of the nine trajectories (Figure S4). Both results support the experimental findings in this work that cyt *c* binds to, or closely associates with, membranes that contain anionic lipids, and does not associate with membranes composed of purely zwitterionic lipids such as DOPC. Additionally, the binding of TOCL to cyt *c* has been reported to occur at different sites (A, L, C, and N) which would lead to different stable orientations at the membrane surface. 40,42,51,59 Thus the observation of two distinctly different binding orientations in the MD trajectories are consistent with experimental observations of cyt *c* interactions with DOPC:TOCL membranes.

Relative Orientation of Cytochrome c Bound to the Bilayers by Simulation Agree with Prior Experimental Studies. The exact location of the anionic phospholipid hosting region(s) in cyt c and therefore, the final orientation(s) of the protein on bilayers containing anionic phospholipids is highly debated. 40,41,51,54-58 We tracked the positions of these regions in each of the trajectories assayed above to determine which orientations are preferred. We find that the effects of bilayer composition on the preferred orientation of cyt c in our simulations correlate directly with experimental observations. 54,56,60 As shown in Figures S5-8, the amino acid site-specific results across the nine MD simulations reveal that bilayers including anionic phospholipid SAPI bind to cyt c with site L nearest to the bilayer surface, while sites A, N, and C are not in contact with the surface. However, when the bilayer includes anionic phospholipid TOCL, two binding orientations are preferred: sites L and A. Previous experimental work has indicated the participation of site A or site L in cyt c binding to cardiolipin. 41,57,61 Interaction sites A and L contain two histidine residues and are rich in lysine, containing seven of the nineteen lysine residues in cyt c. These two binding sites are highly electropositive, containing

about a third of the surface lysine residues, and each basic residue is located on the surface of cyt c. Therefore, interaction between the negatively charged phosphate head group of TOCL and the positive charges of these specific, surface lysine and histidine residues is critical for binding to occur. The existence of two binding orientations in the presence of TOCL suggests a cyt c orientation-specific effect. Each observed orientation of cyt c on the DOPC:TOCL bilayer results in a different face (that is composed of the amino acid residues opposite those involved in the electrostatic binding to the bilayer) being accessible for binding to a nanoparticle and hence can lead to differences in competitive binding. For the bilayer containing SAPI, this corresponds to site A being available for binding to the nanoparticle. For the bilayer containing TOCL, site A or L is available for binding when the cyt c binds at L or A, respectively, though not with equal probability.

Experiment and Simulation. The binding of cyt c to lipid bilayers with high anionic lipid contents can induce conformational perturbations. Au, 63,64 This was not expected for the systems studied here because they contained a maximum of 17.6% TOCL. We conducted circular dichroism and absorbance spectroscopy experiments with free and vesicle-bound cyt c (vesicles with the same phospholipid composition as our QCM-D studies) to confirm the absence of structural perturbations upon lipid binding. We observed no changes in the far- and near-UV regions of the circular dichroism spectra (Figure S13). This indicates that binding to phospholipid vesicles produced no detectable changes in cyt c secondary structure and did not perturb tertiary structure in a manner that discernably influenced the environment and interactions of aromatic side chains. Absorbance spectroscopy focused on the Soret region (350-490 nm) provides information on the spin state of the heme iron. For native cyt c, we observed the expected

maximum absorbance at 410 nm indicating the heme iron has two axial ligands provided by His18 and Met80. 40,66 Comparing native to vesicle-bound cyt c, we observed no changes in either the maximum absorbance or maximum absorbance intensity (Figure S14 and Table S5), indicating no changes in protein conformation that impact the heme iron spin state upon binding to the model biomembranes.

Molecular dynamics simulations confirmed our experimental observations that the secondary and tertiary structures of cyt c were not perturbed upon binding to model biomembranes containing up to 17.6% TOCL. To determine the degree of structural flexibility along the MD simulation trajectories, root mean square deviations (RMSDs) were calculated for the backbone atoms of cyt c (Figure S9). Cytochrome c exhibited relatively low RMSD values during the MD simulations, with deviations remaining ≤ 6 Å. These relatively low RMSD values for backbone cyt c atoms over each trajectory illustrate that the protein retains the majority of its structure during the 200 ns MD simulations. Three trajectories yielded the lowest RMSD values: starting orientations face 1 and face 3 on DOPC:SAPI, and starting orientation face 1 on DOPC:TOCL (Figure S9). To further understand the RMSD fluctuations, the relative mobility of the secondary structure of cyt c induced by the differing bilayer compositions was investigated via STRIDE and VMD.⁶⁷ The PDB structure of cyt c (access code 1AKK) exhibits five α -helical regions involving residues 4-7, 10-15, 51-55, 62-70, and 91-102, a short 3_{10} -helical region encompassing residues 72-74, a β-sheet region spanning 38-39 and 58-59, and several interconnecting turn and coiled regions. Across each MD trajectory, the secondary structural αhelical and β -sheet components were maintained. However, structural transitions from turn to coil or to unstructured conformations were apparent, especially for residues 19-37 (see Figure S9 for visualization of the secondary structure analysis). Overall the secondary structure

components and therefore, shape of cyt c remained mostly unchanged when the protein interacts with bilayers composed of zwitterionic phospholipids and 10 mol% of either of the anionic phospholipids examined. The possible perturbation of cyt c secondary structure due to interaction with ligand-coated nanoparticles is the subject of future work.

Nanoparticle Interaction with Model Biomembranes. We next examined the interaction of 4-5 nm diameter gold nanoparticles (AuNPs) bearing one of two anionic functionalizations: the short molecular ligand mercaptopropionic acid (MPA) or the polymer polyacrylate (PAA) (Figure S15). Several prior studies investigated the interaction of these AuNPs with both supported lipid bilayers and whole organisms. These AuNPs were found to not attach to bilayers composed of solely zwitterionic phospholipids at levels detectable by QCM-D. 17,23 but do interact with cell surfaces of the Gram-negative bacterium Shewanella oneidensis, 68 produce reactive oxygen species in the gut tissue of the microcrustacean Daphnia magna, ⁶⁹ and alter gene expression in S. oneidensis, 70 human fibroblast cells, 71 and D. magna. 69 We determined the hydrodynamic diameters and ζ of these AuNPs in 0.01 M NaCl buffered to pH 7.4 with 0.01 M HEPES by dynamic light scattering and laser Doppler electrophoresis: MPA-AuNPs (9.4 ± 0.5 nm; $\zeta = -43 \pm 4$ mV) and PAA-AuNPs (33 \pm 2 nm; $\zeta = -35 \pm 1$ mV). These data indicate that the MPA-AuNPs are likely not aggregated under the solution conditions employed, whereas the PAA-AuNPs exhibit some degree of aggregation (although they are expected to be slightly larger than the MPA-AuNPs as a result of the layer-by-layer wrapping process used to achieve the anionic polymer coating). We investigated the interaction between these AuNPs and each of the phospholipid bilayers discussed above (viz. DOPC, and DOPC containing 8.8% Liver PI, 4.4% TOCL, 8.8% TOCL, and 17.6% TOCL) in the absence and presence of cyt c by QCM-D.

Anionic mercaptoproprionic acid-functionalized AuNPs. Figure 5A shows representative data for MPA-AuNP attachment to DOPC bilayers, DOPC bilayers containing 4.4 mol% TOCL, and the latter composition with associated cyt c. The MPA-AuNPs did not interact with the pure phospholipid bilayers to an extent detectable by QCM-D, consistent with our previous results for these AuNPs. This lack of interaction was also observed for supported DOPC bilayers containing larger amounts of TOCL (Table S7). In marked contrast, the association of cyt c with model membranes promoted attachment of MPA-AuNPs as indicated by the negative shifts in frequency (representative data in Figure 5A, full data set in Table S7; here we present the data as Δf because $\Delta D/\Delta f > 4 \times 10^{-7}$ Hz⁻¹ and therefore did not support application of the Sauerbrey equation). The interpretation is that cyt c molecules on the membrane surfaces provided local sites of positive charge that led to electrostatic attraction of the anionic nanoparticles and thus their accumulation on the membrane surface, an event not measurable in the absence of cyt c association with the bilayer.

Attachment of MPA-AuNPs differed significantly (p < 0.001) among bilayer types, and appeared to increase with the amount of bound cyt c, suggesting localized nanoparticle attachment to proteins. (The ζ values of the overall bilayer or vesicles containing protein are barely altered, (Table S3) with the exception of the 17.7% TOCL bilayer). Based on the MD simulations described above, cyt c is oriented in TOCL-containing bilayers so that site A or L faces the solution (Figure 6A and B). We hypothesize that the anionic MPA-AuNP interacted with these highly electropositive sites (Figure 6C).

The final change in frequency (Δf_{final}) for MPA-AuNP attachment correlated strongly with the amount of cyt c bound to the bilayer ($R^2 = 0.997$; Figure 5B), indicating that the extent of MPA-AuNPs binding to the bilayer was a function of the amount of cyt c present on the

supported lipid bilayer surface. Interestingly, attachment of MPA-AuNP to the cyt c-coated SiO₂ sensor surface (Figure 5B) does not follow the linear trend for bilayers with bound cyt c. This may indicate differences in cyt c protein structure or orientation when bound to silica vs. a bilayer that increase the favorability of interaction with MPA-AuNPs.

Our results imply that basing the assessment of nanoparticle interaction with cellular membranes solely on interaction with phospholipid bilayers is insufficient. Proteins associated with cellular membranes also contribute to nanoparticle interaction with membranes.

Anionic polyacrylic acid-wrapped AuNPs. We next examined the effect of replacing the short, molecular MPA ligands with the anionic polymer polyacrylic acid. In the absence of cyt c, PAA-AuNPs did not interact with TOCL-containing bilayers to an extent detectable by QCM-D (Figure 5A, Table S7; a small degree of attachment was observed for Liver PI-containing bilayers). In marked contrast and counter to what we observed with the MPA-AuNPs, interaction of PAA-AuNPs with cyt c-containing bilayers produced positive shifts in frequency (Figure 5A; Table S7) corresponding to losses of mass. We attribute the positive frequency shifts to removal of cyt c from the bilayers by the PAA-AuNPs. These data suggest that the energy of interaction between PAA-AuNPs and cyt c exceeds that between the protein and the supported lipid bilayers (as well as that between MPA-AuNPs and cyt c). Free PAA polymers produce the same result: loss of mass of the protein-laden lipid bilayer but no mass loss for lipid bilayers alone (Table S10). One intriguing rationalization of these results is that the binding of PAA-wrapped nanoparticles (but not MPA-conjugated nanoparticles) to cyt c induces a conformational change in the protein that results in a less favorable interaction between the anionic phospholipids and cyt c, which ultimately causes the release of the cyt c-PAA-nanoparticle complex from the surface of the model biomembrane. Presumably the PAA-AuNPs interact with site A or L faced as with the MPA-AuNPs. We illustrate the hypothesized binding of PAA-AuNPs to cyt *c* associated with bilayer surfaces and subsequent removal of the protein from the bilayer in Figure 6D.

The extraction of peripheral membrane proteins from phospholipid bilayers by anionic polymer-wrapped nanoparticles has two important implications. First, our results suggest that the formation of complexes between peripheral membrane proteins and nanoparticles can lead to the incorporation of membrane proteins in the biomolecular corona that often forms on nanoparticles immersed in biological media. Past work has focused on the formation of coronas from soluble proteins. We suggest that the recruitment of membrane proteins into nanoparticle coronas is a fundamental mechanism by which nanoparticles interact with cell or organelle membranes. Second, removal of peripheral membrane proteins from cellular membranes by nanoparticles is another fundamental mechanism by which nanoparticles interact with cellular membranes and produce concomitant impacts on biological function.

The rate and proportion of cyt c that was apparently removed from each bilayer varied as evidenced by differences in the shapes of the Δf traces following PAA-AuNP introduction (data not shown), although the $\Delta f_{\rm final}$ upon interaction of PAA-AuNPs did not differ among supported lipid bilayers with bound cyt c (p > 0.005; Table S7). We determined the initial rate of cyt c removal from the bilayers as described in the Materials and Methods. This analysis revealed a significant (p < 0.001) increase in the initial cyt c removal rate by PAA-AuNPs from supported lipid bilayers containing 4.4% TOCL or 8.8% Liver PI (equivalent amount of anionic lipid charge) relative to those containing 8.8% or 17.6% TOCL. We hypothesize that the rate of removal was related to the strength of cyt c binding to the supported lipid bilayers, which differed by composition. To support this hypothesis, we plotted the initial cyt c removal rates

against the change in fractional coverage of cyt c ($\theta_{\text{cyt}} c$) per unit change in NaCl concentration (Figure 5C). The rate of cyt c removal by the PAA-AuNPs correlated strongly with the strength of cyt c binding to supported lipid bilayers ($R^2 = 0.9308$).

The loss of mass induced by exposure of the cyt c-containing bilayers to PAA-AuNPs does not restore the frequency value to that of the supported lipid bilayers prior to association of cyt c, suggesting that not all bound cyt c was removed from the bilayer. This observation could be explained by the existence of two subpopulations of membrane-bound cyt c, tightly and weakly bound. ^{53,74} In turn, this is consistent with the finding of two possible binding orientations of cyt c relative to the bilayer containing TOCL from the MD trajectories.

CONCLUSIONS

This study demonstrates that membrane-associated proteins can dramatically influence nanoparticle interaction with model biomembranes. The two nanoparticles highlighted here, MPA- and PAA-AuNPs, exhibited no detectable or only limited interaction with supported bilayers composed solely of phospholipids as measured by QCM-D. Strikingly, when the peripheral membrane protein cyt c was associated with bilayers, we observed extensive MPA-AuNP attachment. The extent of attachment scaled with the number of cyt c molecules associated with the bilayers. In contrast, anionic polymer-wrapped gold nanoparticles appeared to remove cyt c from supported lipid bilayers to an extent that was inversely proportional to the strength of cyt c binding to the bilayer. Although all-atom simulations of these systems are highly challenging using current computational resources, we employed a battery of related simulations, varying membrane composition and cyt c orientation, to observe the relative relaxation and orientation of the protein in proximity to the nanoparticle surface. We found that, in apparent consonance with the experiments, inclusion of TOCL in bilayers gave rise to two

possible preferred cyt *c* orientations. We hypothesize that the anionic MPA- and PAA-AuNPs interacted electrostatically with the strongly electropositive sites A and L that face away from the bilayer surface as determined by MD simulations (Figure 6).

While the results in this study were obtained for highly simplified model biomembranes with a single type of protein present at the membrane surface, they clearly indicate that proteins may present high affinity sites for nanoparticle binding, which, as observed in this study, can result in nanoparticle accumulation at the membrane surface or the removal of membrane-bound proteins. Within organisms, this could alter or abolish protein function. Our results thus point to the need to study the impact of nanoparticle exposure on membrane protein function. Supported, tethered, or planar suspended lipid bilayers represent a set of experimental platforms that allow incorporation of membrane proteins (with some important caveats) and that are expected to prove useful in probing nanoparticle interactions with and impacts on membrane proteins. These platforms are amenable to the study of a nanoparticles possessing a wide variety of sizes, shapes and surface functionalities, as well as strongly associated corona proteins. ^{30,98} Mechanistic understanding acquired in such studies would enable more powerful predictions of the potential biological impacts of nanoparticles designed to interact with living systems or present in the environment, and help guide the sustainable development of benign nanoparticles.

MATERIALS AND METHODS

Materials. All materials were used as received, unless otherwise noted. Hydrogen tetrachloroaurate trihydrate (HAuCl₄·3H₂O), sodium borohydride, mercaptopropanoic acid, 3-amino propanethiol hydrochloride, sodium polyacrylate ($M_r = 15~000~Da$, 35 wt % in water), polyallylamine HCl (PAH; $M_r = 15~000~Da$), glycerol (99% purity), and horse heart cyt c were purchased from Sigma Aldrich. Trisodium citrate dihydrate was obtained from Flinn Scientific. We procured HEPES, NaCl, and CaCl₂ from Fisher

Scientific. The phospholipids, 1,2-dioleoyl-sn-glycero-3-phosphocholine, bovine liver α -phosphatidylinositol, and 1',3'-bis[1,2-dioleoyl-sn-glycero-3-phospho]-sn-glycerol were purchased from Avanti Polar Lipids. All aqueous solutions were prepared in ultrapure water (>18 M Ω ·cm). All solutions used were buffered to pH 7.4 with 0.01 M HEPES.

Vesicle and Protein Preparation and Characterization. Small unilamellar vesicles (SUVs) composed of pure DOPC, or DOPC containing 8.8% Liver PI, 4.4% TOCL, 8.8% TOCL, or 17.6% TOCL (all percentages are mol%) were prepared by extrusion as described previously,²³ with the exception that the hydration solution was 0.001 M NaCl and the stock vesicle concentration was 2.5 g·L⁻¹. The SUVs were stored at 4 °C and used within 1 week. Cytochrome c stock solution (1 g·L⁻¹) was prepared in 0.01 M NaCl and stored at -20 °C.

Vesicle hydrodynamic diameter (d_h) and ζ of SUVs were determined by dynamic light scattering and laser Doppler electrophoresis (Malvern Zetasizer Nano ZS) using SUV suspensions (0.0625 g·L⁻¹) in 0.01 M NaCl that had been vortexed for 15 s. Reported d_h (number mean) and ζ values represent averages of six measurements each consisting of 10 or 20 runs, respectively. The effect of cyt c binding on vesicle d_h and ζ was determined using SUV suspensions that had been gently mixed by pipetting with 0.02, 0.04, 0.08, or 0.16 g·L⁻¹ cyt c.

We examined structural changes to cyt c induced by binding to SUVs by circular dichroism and absorbance spectra in the Soret region (350-490 nm). Circular dichroism spectra in the far- and near-UV regions were collected for 10 μ M cyt c in the presence and absence of 10 mM SUVs. Cytochrome c spectra in the presence of SUVs were background subtracted using the spectra of the vesicles alone. Far-UV and near-UV spectra were measured in 1 mm and 10 mm quartz cuvettes, respectively. Spectra were obtained with a 50 nm·min⁻¹ scan rate, 1 nm bandwidth, and 1 nm spectral resolution, and represent the averages of four scans. Absorbance spectra were obtained for 5 μ M cyt c in the absence and presence of 0.5 mM vesicles, and the spectra of lipid-protein complexes was background subtracted using the spectra of SUVs alone.

Nanoparticle Synthesis and Characterization. Gold nanoparticles (4-5 nm core diameter) were prepared by borohydride reduction of HAuCl₄ in the presence of MPA or citrate, as previously described. The resulting MPA-AuNP solution was purified by diafiltration. Citrate-AuNPs were wrapped with PAH and purified by diafiltration, followed by centrifugation and washing. PAA-wrapped AuNPs were prepared from the PAH-AuNPs and purified by diafiltration, followed by centrifugation. Nanoparticle concentrations were determined by UV-visible spectroscopy using a known extinction coefficient. Gold nanoparticle suspensions were diluted to 10 nM in 0.01 M NaCl solution, vortexed for 15 s, and their d_h and ζ were determined as described above for the SUVs.

Quartz Crystal Microbalance with Dissipation Monitoring. We employed QCM-D to monitor supported lipid bilayer formation, cyt c attachment to supported lipid bilayers, and the interaction of nanoparticles with supported lipid bilayers in the absence and presence of cyt c. Quartz crystal microbalance with dissipation monitoring measures changes in the resonance frequency (Δf) and energy dissipation (ΔD) induced by interaction of an analyte with the surface of a coated (SiO₂ or Si₃N₄ in the present study) piezoelectric quartz crystal. Changes in frequency reflect changes in the acoustic mass coupled to the sensor surface (analyte mass and dynamically coupled solvent). Changes in energy dissipation are related to the viscoelastic properties of laterally homogenous adlayers or the rigidity of the particle-surface contact region for films of discrete nanoscale objects.⁷⁹ In the case of a rigidly coupled adlayer ($\Delta D_v/(-\Delta f_v/v) \ll 0.4 \times 10^{-6} \text{ Hz}^{-1}$, where v is the harmonic number),⁴⁷ the Sauerbrey relationship⁴⁶ can be used to estimate the change in acoustic surface mass density ($\Delta \Gamma_{OCM-D}$):

$$\Delta\Gamma_{\text{QCM-D}} = -C \frac{\Delta f_{\nu}}{\nu} \tag{1}$$

where C is the mass sensitivity constant (18 ng·cm⁻²·Hz⁻¹ at the fundamental frequency, $f_1 = 4.95$ MHz).

All experiments were conducted at a 0.1 mL·min⁻¹ flow rate (except during protein attachment to the supported bilayer surface, noted below) and 25 °C. All experiments using conventional QCM-D sensors were conducted using the Q-Sense E4 system (Biolin Scientific, Göteborg, Sweden) containing silicacoated sensors (QSX 303) mounted in temperature-controlled liquid flow cells (QFM 401). QCM-D

sensor crystals were prepared for use by bath sonication in 2% (w/v) sodium dodecyl sulfate for 20 min, rinsing extensively and consecutively with ultrapure water, ethanol, and ultrapure water; drying with a stream of N_2 gas; and UV/ozone treatment for 30 min (Bioforce Nanosciences UV/Ozone Procleaner) immediately prior to mounting in the flow cells. Supported lipid bilayers were formed by vesicle fusion. Heriefly, after stabilizing sensor frequency and dissipation response under flow of a solution composed of 0.15 M NaCl and 0.005 M CaCl₂, we flowed SUVs (0.125 mg·mL⁻¹ in the same solution) across the sensors until the Δf and ΔD values passed through a minimum and maximum, respectively, that indicate attainment of the critical adsorbed vesicle concentration and commencement of vesicle fusion and rupture leading to the spontaneous formation of a supported lipid bilayer. The supported lipid bilayer was rinsed sequentially with vesicle-free solution of the same composition (~5 min), 0.15 M NaCl (~5 min), and 0.01 M NaCl (~10 min). The duration of each rinse period was dictated by the attainment of stable Δf and ΔD values.

For experiments investigating the influence of cyt c on nanoparticle interaction with model biomembranes, protein solution (0.05 mg·mL⁻¹) in 0.01 M NaCl was flowed over the bilayer for 20 min at a reduced flow rate of 0.05 mL·min⁻¹. After 30 min, the flow was halted for 30 min. After this period, flow was increased to 0.1 mL·min⁻¹ and protein-free solution was flowed over the sensor for 10 min to remove any weakly adsorbed protein. In a sub-set of experiments, the strength of cyt c attachment to supported lipid bilayers was assessed by incrementally increasing solution ionic strength and monitoring protein detachment from the bilayer. In these experiments, the NaCl concentration was increased from 0.01 to 0.1 M in 0.01 M increments (10 min for each increment), with each increment followed by a 10 min rinse with 0.01 M NaCl. For cases in which cyt c remained adsorbed to the bilayer surface at 0.1 M NaCl, the salt concentration was increased to 0.15 M for 10 min followed by a 10 min rinse with 0.01 M

After formation of (cyt c-containing) supported lipid bilayers, we flowed 10 nM nanoparticle suspensions in 0.01 M NaCl over the model biomembranes for 20 min to determine how the presence of cyt c altered the interaction of nanoparticles with the supported lipid bilayer system. After the 20-min

period nanoparticle-free solution was flowed for 20 min to assess the reversibility of changes in Δf and ΔD .

Nanoplasmonic Sensing. Nanoplasmonic sensing in reflection mode was conducted using a QCM-D sensor crystal decorated with 100 nm diameter nanoplasmonic gold discs coated with ~10 nm Si_3N_4 . Coupling of light delivered via a fiber optic cable induces charge density oscillations in the gold discs, producing localized surface plasmon resonance (LSPR).⁸⁰ The wavelength of maximum extinction (λ_{max}) is sensitive to the local refractive index. Monitoring $\Delta\lambda_{max}$ induced by the change in local refractive index due to analyte adsorption allows optical mass to be determined.

Nanoplasmonic sensing experiments were conducted using a combined NPS and QCM-D setup that was comprised of a QSense E4 system equipped with a window module (QWM401) connected to an Insplorion Acoulyte. The Acoulyte sensors were QCM-D chips modified with a gold nanodisk array on the sensing surface overcoated with Si_3N_4 (10 nm; ACO-SEN1Insplorion). Prior to use, Acoulyte sensors were treated with UV/ozone for 10-15 min to oxidize the surface and produce a thin SiO_2 layer. Formation of supported lipid bilayers and incorporation of cyt c into them was accomplished as described above in the section on QCM-D.

The change in optical surface mass density, $\Delta\Gamma_{LSPR}$, can be estimated from the de Feijter formula ^{82,83}

$$\Delta\Gamma_{\rm LSPR} \approx \frac{t \left(n_{\rm film} - n_{\rm buffer} \right)}{dn/dC}$$
 (2)

where t is adlayer thickness, n_{film} and n_{buffer} are the refractive indices of the adlayer and buffer, and dn/dC is the refractive index increment. The pairing of NPS with QCM-D allows simultaneous determination of optical ("dry") and acoustic ("wet") mass associated with the sensor surface. Details are provided in the Supporting Information (SI).

Analysis of QCM-D and LSPR Data. We converted the QCM-D frequency data for supported lipid bilayers and incorporation cyt c to acoustic mass using the Sauerbrey model.⁴⁶ The frequency and dissipation responses for the nanoparticle attachment experiments were such that the Sauerbrey model could not be applied $((\Delta D_v/(-\Delta f_v/v) > 0.4 \times 10^{-6} \text{ Hz}^{-1})^{47}$ and changes in frequency are instead reported. For

the LSPR data, $\Delta\lambda_{\text{max}}$ was used to calculate optical mass⁸² as detailed in the SI. Reported frequency, dissipation, and surface mass densities represent averages of at least triplicate measurements. To calculate initial rates of cyt c removal from or nanoparticle deposition to supported lipid bilayers, the raw QCM-D frequency data were subjected to locally weighted scatterplot smoothing with a smoothing parameter of 0.03. We determined the slope between each QCM-D data point (one data point every ~1.3 s) and averaged the slopes of the initial 30 s of nanoparticle attachment or cyt c removal to determine the initial rate of deposition or removal.

Molecular Dynamics (MD) Simulations. A challenge for characterizing nanoparticles and membrane proteins on bilayers using computational models lies in the simultaneous relevance of many length scales: those associated with the nanoparticle structure, the nanoparticle surface, the relative distances of the nanoparticle and protein to the bilayer, and the even larger lengths of the bilayer. In this work, we exploit the increasing power of computers to propagate all-atom MD simulations of relatively large systems at long times⁸⁴ by focusing on the smaller system consisting of only a membrane protein and a bilayer surface to infer the possible points of contact to a nanoparticle.

Selection of Cyt c Starting Orientations on Model Bilayer Surfaces. Figure 1 shows the adaptive Poisson-Boltzmann electrostatic potential of the cyt c surface in three orientations to highlight the nearly completely electropositive nature of face 1 and the mixture of positively and negatively charged regions on faces 2 and 3. Face 1 was chosen to direct the electropositive heme group toward the bilayer surface. Amino acid residues 16-28 and 76-84 comprise the majority of this face, and we use these residues to calculate the Face 1 COM. Face 1 partially overlaps the electrostatic binding site L and shares no amino acids with sites A, C, or N. However, site A is in close proximity to face 1. A 90° rotation of this structure (around an axis so-defined) results in 19 amino acid residues (20-27, 29-33, and 42-47) in proximity to the bilayer; these residues comprise face 2. Faces 1 and 2 overlap, sharing some amino acid residues; both faces include residues found in the acidic phospholipid binding site L. Face 2 is farther from site A than is face 1, and therefore closer to the residues that comprise binding sites C and N. A further 90° rotation about the same axis results in the unique orientation where face 1, dominated by the electropositive heme

group, is oriented opposite to the bilayer surface. The resulting face 3 in closest proximity to the bilayer consists of 21 amino acid residues (61-74 and 86-92). Face 3 is composed of residues that overlap site A and are near site N, but not sites C and L. Figure 3 illustrates the three bilayers considered in this study with the three respective faces of cyt c physisorbed onto the surface.

Atomistic System Construction. All bilayer components were constructed and assembled for the MD simulations using the CHARMM GUI Membrane Builder (http://www.charmm-gui.org/).85,86 The homogeneous bilayer was composed of 100% DOPC and the two heterogeneous bilayers were composed of DOPC:SAPI and DOPC:TOCL in 9:1 ratios. The protonation states of SAPI and TOCL were taken such that each molecule bore a charge of -1 or -2, respectively. In Figure 3, each bilayer is represented through a periodic patch of approximately 120 Å × 120 Å in the plane of the bilayer. We distributed the SAPI and TOCL uniformly in the two bilayer leaflets in equal proportions. We note that actual mitochondrial membranes are unlikely to have equal numbers of anionic lipids in both leaflets due to the presence of many other molecular components. Furthermore, we recognize that the outer and inner leaflet environments differ substantially. However, in the absence of these known constraints, unequal distribution of lipids across the bilayer might induce artificial elements in the simulation with unknown implications.⁸⁷ Moreover, the anionic lipid TOCL comprises ~10 mol% of the inner mitochondrial membrane.⁸⁸ The 9:1 leaflet compositions used in the MD simulations closely match the bilayer compositions used in the experiments reported herein. The protein and bilayer were combined using the visualization and analysis program VMD.⁸⁹ The protein was positioned on the plane of the bilayer surface in one of the three starting orientations chosen so that the selected face (shown in Figure 3) of the protein is oriented towards the bilayer as illustrated in Figure 1. The resulting nine systems (three orientations over each of three bilayer compositions) were solvated with all-atom TIP3P water⁹⁰ up to 100 Å above (where cyt c is also solvated) and down to 30 Å below the bilayer. Periodic boundary conditions were employed between the faces of the resulting periodic box. The charges were neutralized, and the system was ionized to 0.01 M NaCl.

Simulation Methods and Parameters. All initially constructed bilayers were minimized and equilibrated in an ionized periodic TIP3P solvent box prior to production simulations with cyt c. This mitigates the small but non-negligible effect of lipid packing on the preferred orientations of cyt c. The initial minimization and equilibration also relaxes the uncorrelated bilayer components through a series of stages successively releasing constraints on water, ions, and lipid bilayer. To address similar concerns about the cyt c (1AKK) structure and to remove bad contacts, the protein was initially energy-minimized in an ionized TIP3P periodic box. The protein then underwent a series of successively less constrained relaxations to the point when it was unconstrained and free to equilibrate inside the TIP3P periodic box for tens of nanoseconds in the final relaxation. Only after both system components (protein and bilayer) were minimized and equilibrated separately, were the two components combined to make each of the systems of interest. These combined systems were re-solvated, re-ionized, and then minimized and equilibrated following a series of successively less constrained relaxations following the same protocol as above. After the final mostly free equilibration was completed, distance constraints on cyt c were released to propagate the combined system through MD trajectories at constant number, pressure and temperature.

Trajectories starting from the prepared initial systems were propagated in the NPT ensemble with a 2-fs time step for 10⁸ steps (i.e., 200 ns simulation per system totaling 1.8 μs simulation time). Simulations were run using the MD program NAMD 2.11⁹¹ and the CHARMM force field.⁹²⁻⁹⁵ Periodic boundary conditions were applied to all dimensions, and temperature and pressure were fixed to 303.15 K and 1 atm. Pressure was constrained using the Langevin piston algorithm, and temperature was constrained with a damping coefficient of 1.⁹⁶ The particle-mesh Ewald approximation⁹⁷ was employed to account for the long-range electrostatic interactions, while the short-ranged Lennard-Jones and Coulombic interactions were truncated smoothly by a 12 Å cutoff with a switching function applied beyond 10 Å. The cutoff distance for the hydrogen bonding profiles was 3 Å between the potential donor and acceptor atoms, with a 20° angular cutoff.

ASSOCIATED CONTENT

Supporting Information

The Supporting Information is available free of charge on the ACS Publications website at DOI: 10.1021/acs.langmuir.#######.

Further details on nanoplasmonic sensing and molecular dynamics experiments and analysis, QCM-D and nanoplasmonic sensing data, DLS/ ζ potential data, molecular dynamics simulation data, and UV-Vis and CD analysis of lipid vesicle-bound cytochrome c.

AUTHOR INFORMATION

Corresponding Authors

* E-mail: joelpedersen@wisc.edu * E-mail: r.hernandez@jhu.edu

ORCID

Eric S. Melby: 0000-0002-3812-2965

Isabel U. Foreman-Ortiz: 0000-0003-3169-7026

Emily R. Caudill: 0000-0002-3645-9804

Catherine J. Murphy: 0000-0001-7066-5575

Rigoberto Hernandez: 0000-0001-7066-5575

Joel A. Pedersen: 0000-0002-3918-1860

Author Contributions

E.S.M. and C.A. contributed equally to this work. E.S.M., C.A., R.H., and J.A.P. designed research; E.S.M, I.U.F.-O., E.R.C., and T.R.K. performed research; C.A. conducted molecular dynamics simulations; A.M.V., X.Z., and C.J.M contributed new reagents/analytical tools; E.S.M., C.A., I.U.F.-O.; E.R.C., C.A., R.H. and J.A.P. analyzed data; E.S.M., C.A., I.U.F.-O., C.J.M., R.H., and J.A.P. wrote the manuscript.

Notes

The authors declare no competing financial interests.

ACKNOWLEDGMENTS

This work was supported by National Science Foundation under the Center for Sustainable Nanotechnology, CHE-1503408. The CSN is part of the Centers for Chemical Innovation Program. The computing resources necessary for this research were provided in part by the NSF through XSEDE resources provided by Comet (TG-CTS090079), and by the Maryland Advanced Research Computing Center (MARCC). J.A.P. gratefully acknowledges support from the William A. Rothermel–Bascom Professorship. We thank Jennifer Andersson (Insplorion) for helpful discussions. A portion of the research was performed using the Environmental Molecular Sciences Laboratory, a DOE Office of Science User Facility sponsored by the Office of Biological and Environmental Research and located at the Pacific Northwest National Laboratory.

ABBREVIATIONS. cyt c, cytochrome c; DOPC, 18:1 phosphatidylcholine; Liver PI, mixture of phosphatidylinositol lipids; TOCL, 18:1 cardiolipin; MD, molecular dynamics; QCM-D, quartz crystal microbalance with dissipation monitoring; Δf , change in frequency; ΔD , change in dissipation; NPS, nanoplasmonic sensing; LSPR, localized surface plasmon resonance; SAPI, 18:0-20:4-phosphoinositol; COM, center of mass; RMSD, root mean square deviations; AuNP, gold nanoparticle; MPA, mercaptopropanoic acid; PAA, polyacrylic acid; SUV, small unilamellar vesicle; d_h , hydrodynamic diameter; ζ , zeta potential; CD, circular dichroism.

REFERENCES

- (1) Murphy, C. J., Vartanian, A. M., Geiger, F. M., Hamers, R. J., Pedersen, J., Cui, Q., Haynes, C. L., Carlson, E. E., Hernandez, R., Klaper, R. D., Orr, G., and Rosenzweig, Z. (2015) Biological Responses to Engineered Nanomaterials: Needs for the Next Decade. *ACS Cent. Sci.* 1, 117–123.
- (2) Nel, A. E., Mädler, L., Velegol, D., Xia, T., Hoek, E. M. V, Somasundaran, P., Klaessig, F., Castranova, V., and Thompson, M. (2009) Understanding biophysicochemical interactions at the nanobio interface. *Nat. Mater.* 8, 543–557.
- (3) Dogangun, M., Hang, M. N., Troiano, J. M., Mcgeachy, A. C., Melby, E. S., Pedersen, J. A., Hamers, R. J., and Geiger, F. M. (2015) Alteration of Membrane Compositional Asymmetry by LiCoO₂ Nanosheets. *ACS Nano* 9, 8755–8765.
- (4) Berry, C. C., and Curtis, A. S. (2003) Functionalization of magnetic nanoparticles for applications in biomedicine. *J. Phys. D. Appl. Phys.* 36, 198–206.
- (5) Verma, A., and Stellacci, F. (2010) Effect of surface properties on nanoparticle-cell interactions. *Small* 6, 12–21.
- (6) Zhang, S., Gao, H., and Bao, G. (2015) Physical Principles of Nanoparticle Cellular Endocytosis. *ACS Nano 9*, 8655–8671.
- (7) Hong, S., Leroueil, P. R., Janus, E. K., Peters, J. L., Kober, M. M., Islam, M. T., Orr, B. G., Baker, J. R., and Banaszak Holl, M. M. (2006) Interaction of polycationic polymers with supported lipid bilayers and cells: Nanoscale hole formation and enhanced membrane permeability. *Bioconjug. Chem.* 17, 728–734.
- (8) Leroueil, P. R., Hong, S., Mecke, A., Baker, J. R., Orr, B. G., and Banaszak Holl, M. M. (2007) Nanoparticle interaction with biological membranes: does nanotechnology present a Janus face? *Acc. Chem. Res.* 40, 335–42.
- (9) Zhu, W., von dem Bussche, A., Yi, X., Qiu, Y., Wang, Z., Weston, P., Hurt, R., Kane, A., and Gao, H.

- (2016) Nanomechanical mechanism for lipid bilayer damage induced by carbon nanotubes confined in intracellular vesicles. *Proc. Natl. Acad. Sci. 113*, 12374–12379.
- (10) Tu, Y., Lv, M., Xiu, P., Huynh, T., Zhang, M., Castelli, M., Liu, Z., Huang, Q., Fan, C., Fang, H., and Zhou, R. (2013) Destructive extraction of phospholipids from Escherichia coli membranes by graphene nanosheets. *Nat. Nanotechnol.* 8, 594–601.
- (11) van Meer, G., Voelker, D. R., and Feigenson, G. W. (2008) Membrane lipids: where they are and how they behave. *Nat. Rev. Mol. Cell Biol.* 9, 112–24.
- (12) Luckey, M. (2014) Membrane Structural Biology with Biochemical and Biophysical Foundations 2nd ed. Cambridge University Press, Cambridge, UK.
- (13) Van Lehn, R. C., Ricci, M., Silva, P. H. J., Andreozzi, P., Reguera, J., Voïtchovsky, K., Stellacci, F., and Alexander-Katz, A. (2014) Lipid tail protrusions mediate the insertion of nanoparticles into model cell membranes. *Nat. Commun. 5*, 4482.
- (14) Carney, R. P., Astier, Y., Carney, T. M., Voïtchovsky, K., Jacob Silva, P. H., and Stellacci, F. (2013) Electrical method to quantify nanoparticle interaction with lipid bilayers. *ACS Nano* 7, 932–942.
- (15) Yi, P., and Chen, K. L. (2013) Interaction of multiwalled carbon nanotubes with supported lipid bilayers and vesicles as model biological membranes. *Environ. Sci. Technol.* 47, 5711–5719.
- (16) Liu, X., and Chen, K. L. (2015) Interactions of graphene oxide with model cell membranes: Probing nanoparticle attachment and lipid bilayer disruption. *Langmuir 31*, 12076–12086.
- (17) Troiano, J. M., Olenick, L. L., Kuech, T. R., Melby, E. S., Hu, D., Lohse, S. E., Mensch, A. C., Dogangun, M., Vartanian, A. M., Torelli, M. D., Ehimiaghe, E., Walter, S. R., Fu, L., Anderton, C. R., Zhu, Z., Wang, H., Orr, G., Murphy, C. J., Hamers, R. J., Pedersen, J. A., and Geiger, F. M. (2015) Direct Probes of 4 nm Diameter Gold Nanoparticles Interacting with Supported Lipid Bilayers. *J. Phys. Chem. C* 119, 534–546.
- (18) Yousefi, N., Wargenau, A., and Tufenkji, N. (2016) Toward More Free-Floating Model Cell Membranes: Method Development and Application to Their Interaction with Nanoparticles. *ACS Appl. Mater. Interfaces* 8, 14339–14348.
- (19) Chen, J., Hessler, J. A., Putchakayala, K., Panama, B. K., Khan, D. P., Hong, S., Mullen, D. G., DiMaggio, S. C., Som, A., Tew, G. N., Lopatin, A. N., Baker, J. R., Banaszak Holl, M. M., and Orr, B. G. (2009) Cationic nanoparticles induce nanoscale disruption in living cell plasma membranes. *J. Phys. Chem. B* 113, 11179–11185.
- (20) Lin, J., Zhang, H., Chen, Z., and Zheng, Y. (2010) Penetration of Lipid Membranes by Gold Nanoparticles: Insights into Cellular Uptake, Cytotoxicity, and Their Relationships. *ACS Nano 4*, 5421–5429.
- (21) Zhang, X., and Yang, S. (2011) Nonspecific Adsorption of Charged Quantum Dots on Supported Zwitterionic Lipid Bilayers: Real-Time Monitoring by Quartz Crystal Microbalance with Dissipation. *Langmuir* 27, 2528–2535.
- (22) Lin, J.-Q., Zheng, Y.-G., Zhang, H.-W., and Chen, Z. (2011) A simulation study on nanoscale holes generated by gold nanoparticles on negative lipid bilayers. *Langmuir 27*, 8323–32.
- (23) Melby, E. S., Mensch, A. C., Lohse, S. E., Hu, D., Orr, G., Murphy, C. J., Hamers, R. J., and Pedersen, J. A. (2016) Formation of supported lipid bilayers containing phase-segregated domains and their interaction with gold nanoparticles. *Environ. Sci. Nano* 3, 45–55.
- (24) Jacobson, K. H., Gunsolus, I. L., Kuech, T. R., Troiano, J. M., Melby, E. S., Lohse, S. E., Hu, D., Chrisler, W. B., Murphy, C. J., Orr, G., Geiger, F. M., Haynes, C. L., and Pedersen, J. A. (2015) Lipopolysaccharide Density and Structure Govern the Extent and Distance of Nanoparticle Interaction with Actual and Model Bacterial Outer Membranes. *Environ. Sci. Technol.* 49, 10642–10650.
- (25) Stevens, T. J., and Arkin, I. T. (2000) Do more complex organisms have a greater proportion of membrane proteins in their genomes? *Proteins Struct. Funct. Genet.* 39, 417–420.
- (26) Almén, M., Nordström, K. J., Fredriksson, R., and Schiöth, H. B. (2009) Mapping the human membrane proteome: a majority of the human membrane proteins can be classified according to function and evolutionary origin. *BMC Biol.* 7, 50.
- (27) Cedervall, T., Lynch, I., Lindman, S., Berggård, T., Thulin, E., Nilsson, H., Dawson, K. A., and

- Linse, S. (2007) Understanding the nanoparticle-protein corona using methods to quantify exchange rates and affinities of proteins for nanoparticles. *Proc. Natl. Acad. Sci. U. S. A. 104*, 2050–2055.
- (28) Lundqvist, M., Stigler, J., Elia, G., Lynch, I., Cedervall, T., and Dawson, K. A. (2008) Nanoparticle size and surface properties determine the protein corona with possible implications for biological impacts. *Proc. Natl. Acad. Sci. U. S. A. 105*, 14265–14270.
- (29) Walkey, C. D., Olsen, J. B., Song, F., Liu, R., Guo, H., Olsen, D. W. H., Cohen, Y., Emili, A., and Chan, W. C. W. (2014) Protein Corona Fingerprinting Predicts the Cellular Interaction of Gold and Silver Nanoparticles. *ACS Nano* 8, 2439–2455.
- (30) Melby, E. S., Lohse, S. E., Park, J. E., Vartanian, A. M., Putans, R. A., Abbott, H. B., Hamers, R. J., Murphy, C. J., and Pedersen, J. A. (2017) Cascading Effects of Nanoparticle Coatings: Surface Functionalization Dictates the Assemblage of Complexed Proteins and Subsequent Interaction with Model Cell Membranes. *ACS Nano 11*, 5489–5499.
- (31) Orr, G., Panther, D. J., Cassens, K. J., Phillips, J. L., Tarasevich, B. J., and Pounds, J. G. (2009) Syndecan-1 mediates the coupling of positively charged submicrometer amorphous silica particles with actin filaments across the alveolar epithelial cell membrane. *Toxicol. Appl. Pharmacol.* 236, 210–220.
- (32) Zhang, H., Xia, T., Meng, H., Xue, M., George, S., Ji, Z., Wang, X., Liu, R., Wang, M., France, B., Rallo, R., Damoiseaux, R., Cohen, Y., Bradley, K. A., Zink, J. I., and Nel, A. E. (2011) Differential Expression of Syndecan-1 Mediates Cationic Nanoparticle Toxicity in Undifferentiated versus Differentiated Normal Human Bronchial Epithelial Cells. *ACS Nano* 5, 2756–2769.
- (33) Gu, Z., Plant, L. D., Meng, X.-Y., Perez-Aguilar, J. M., Wang, Z., Dong, M., Logothetis, D. E., and Zhou, R. (2017) Exploring the Nanotoxicology of MoS2: A Study on the Interaction of MoS2 Nanoflakes and K + Channels. *ACS Nano* 10.1021/acsnano.7b07871.
- (34) Wu, L., and Jiang, X. (2016) Recent developments in methodology employed to study the interactions between nanomaterials and model lipid membranes. *Anal. Bioanal. Chem.* 408, 2743–2758.
- (35) Chen, K., and Bothun, G. (2014) Nanoparticles Meet Cell Membranes: Probing Nonspecific Interactions using Model Membranes. *Environ. Sci. Technol.* 48, 873–880.
- (36) Contini, C., Schneemilch, M., Gaisford, S., and Quirke, N. (2018) Nanoparticle-membrane interactions. *J. Exp. Nanosci.* 13, 62–81.
- (37) Tatur, S., and Badia, A. (2012) Influence of Hydrophobic Alkylated Gold Nanoparticles on the Phase Behavior of Monolayers of DPPC and Clinical Lung Surfactant. *Langmuir 28*, 628–639.
- (38) Beck-Broichsitter, M., Ruppert, C., Schmehl, R., Günther, A., and Seeger, W. (2014) Biophysical inhibition of synthetic vs. naturally-derived pulmonary surfactant preparations by polymeric nanoparticles. *Elsevier 1838*, 474–481.
- (39) MacCormack, T. J., Rundle, A. M., Malek, M., Raveendran, A., and Meli, M.-V. (2017) Gold nanoparticles partition to and increase the activity of glucose-6-phosphatase in a synthetic phospholipid membrane system. *PLoS One* (Kursula, P., Ed.) *12*, e0183274.
- (40) Tuominen, E. K. J., Wallace, C. J. A., and Kinnunen, P. K. J. (2002) Phospholipid-Cytochrome c Interaction: Evidence for the Extended Lipid Anchorage. *J. Biol. Chem.* 277, 8822–8826.
- (41) Kalanxhi, E., and Wallace, C. J. A. (2007) Cytochrome c impaled: investigation of the extended lipid anchorage of a soluble protein to mitochondrial membrane models. *Biochem. J* 407, 179–187.
- (42) Hannibal, L., Tomasina, F., Capdevila, D. A., Demicheli, V., Tórtora, V., Alvarez-Paggi, D., Jemmerson, R., Murgida, D. H., and Radi, R. (2016) Alternative Conformations of Cytochrome *c*: Structure, Function, and Detection. *Biochemistry* 55, 407–428.
- (43) Reed, J. (1997) Cytochrome c: can't live with it-can't live without it. Cell 91, 559–562.
- (44) Cho, N.-J., Frank, C. W., Kasemo, B., and Höök, F. (2010) Quartz crystal microbalance with dissipation monitoring of supported lipid bilayers on various substrates. *Nat. Protoc.* 5, 1096–106.
- (45) Richter, R. P., Berat, R., and Brisson, A. R. (2006) Formation of Solid-Supported Lipid Bilayers: An Integrated View. *Langmuir 22*, 3497–3505.
- (46) Sauerbrey, G. (1959) Verwendung von Schwingquarzen zur Wägung dünner Schichten und zur Mikrowägung. Zeitschrift für Phys. 155, 206–222.
- (47) Reviakine, I., Johannsmann, D., and Richter, R. P. (2011) Hearing what you cannot see and

- visualizing what you hear: Interpreting quartz crystal microbalance data from solvated interfaces. *Anal. Chem. 83*, 8838–8848.
- (48) Glasmästar, K., Larsson, C., Höök, F., and Kasemo, B. (2002) Protein adsorption on supported phospholipid bilayers. *J. Colloid Interface Sci.* 246, 40–7.
- (49) Barlow, G. H., and Margoliash, E. (1966) Electrophoretic behavior of mammalian-type cytochromes c. *J. Biol. Chem.* 241, 1473–1477.
- (50) Rytömaa, M., Mustonen, P., and Kinnunen, P. K. J. (1992) Reversible, nonionic, and pH-dependent association of cytochrome c with cardiolipin-phosphatidylcholine liposomes. *J. Biol. Chem.* 267, 22243–22248.
- (51) Rytömaa, M., and Kinnunen, P. K. J. (1995) Reversibility of the binding of cytochrome c to liposomes: Implications for lipid-protein interactions. *J. Biol. Chem.* 270, 3197–3202.
- (52) Zimmermann, R., Küttner, D., Renner, L., Kaufmann, M., Zitzmann, J., Müller, M., and Werner, C.
- (2009) Charging and structure of zwitterionic supported bilayer lipid membranes studied by streaming current measurements, fluorescence microscopy, and attenuated total reflection Fourier transform infrared spectroscopy. *Biointerphases 4*, 1–6.
- (53) Cortese, J. D., Voglino, A. L., and Hackenbrock, C. R. (1998) Multiple conformations of physiological membrane-bound cytochrome c. *Biochemistry* 37, 6402–6409.
- (54) Rytömaa, M., and Kinnunen, P. K. J. (1994) Evidence for two distinct acidic phospholipid-binding sites in cytochrome c. *J. Biol. Chem.* 269, 1770–1774.
- (55) Kinnunen, P. K., Kõiv, A., Lehtonen, J. Y., Rytömaa, M., and Mustonen, P. (1994) Lipid dynamics and peripheral interactions of proteins with membrane surfaces. *Chem. Phys. Lipids* 73, 181–207.
- (56) O'Brien, E. S., Nucci, N. V, Fuglestad, B., Tommos, C., and Wand, A. J. (2015) Defining the Apoptotic Trigger: The Interaction of Cytochrome c and Cardiolipin. *J. Biol. Chem.* 52, 4578–4588.
- (57) Kawai, C., Prado, F. M., Nunes, G. L. C., Di Mascio, P., Carmona-Ribeiro, A. M., Nantes, I. L., Mascio, P. Di, Carmona-Ribeiro, A. M., and Nantes, I. L. (2005) pH-Dependent interaction of cytochrome c with mitochondrial mimetic membranes: the role of an array of positively charged amino acids. *J. Biol. Chem.* 280, 34709–34717.
- (58) Sinibaldi, F., Howes, B. D., Droghetti, E., Polticelli, F., Maria, ∥, Piro, C., Donato, ⊥, Pierro, D., Fiorucci, L., Coletta, M., Smulevich, G., and Santucci, R. (2013) Role of Lysines in Cytochrome c–Cardiolipin Interaction. *Biochemistry* 52, 4578–4588.
- (59) Sinibaldi, F., Howes, B. D., Piro, M. C., Polticelli, F., Bombelli, C., Ferri, T., Coletta, M., Smulevich, G., and Santucci, R. (2010) Extended cardiolipin anchorage to cytochrome c: A model for protein-mitochondrial membrane binding. *J. Biol. Inorg. Chem.* 15, 689–700.
- (60) Vladimirov, Y. A., Proskurnina, E. V, and Alekseev, A. V. (2013) Molecular Mechanisms of Apoptosis. Structure of Cytochrome c Cardiolipin Complex. *Biochemistry* 78, 1086–1097.
- (61) Kostrzewa, A., Páli, T., Froncisz, W., and Marsh, D. (2000) Membrane Location of Spin-Labeled Cytochrome c Determined by Paramagnetic Relaxation Agents. *Biochemistry* 39, 6066–6074.
- (62) Kagan, V., Bayir, H., Belikova, N., Kapralov, O., Tyurina, Y. Y., Tyurin, V. A., Jiang, J., Stoyanovsky, D., Wipf, P., Kochanek, P., Greenberger, J., Pitt, B., Svedova, A., and Borisenko, G. G. (2009) Cytochrome c/cardiolipin relations in mitochondria: a kiss of death. *Free Radic. Biol. Med.* 46, 1439–1453.
- (63) Spooner, P. J. R., and Watts, A. (1992) Cytochrome c interactions with cardiolipin in bilayers: A multinuclear magic-angle spinning NMR study. *Biochemistry 31*, 10129–10138.
- (64) Muga, A., Mantsch, H. H., and Surewicz, W. K. (1991) Membrane binding induces destabilization of cytochrome c structure. *Biochemistry* 30, 7219–24.
- (65) Kelly, S. M., Jess, T. J., and Price, N. C. (2005) How to study proteins by circular dichroism. *Biochim. Biophys. Acta Proteins Proteomics* 1751, 119–139.
- (66) Sanghera, N., and Pinheiro, T. J. T. (2000) Unfolding and refolding of cytochrome c driven by the interaction with lipid micelles. *Protein Sci. 9*, 1194–1202.
- (67) Heinig, M., and Frishman, D. (2004) STRIDE: a web server for secondary structure assignment from known atomic coordinates of proteins. *Nucleic Acids Res. 32*, W500-502.

- (68) Feng, Z. V., Gunsolus, I. L., Qiu, T. A., Hurley, K. R., Nyberg, L. H., Frew, H., Johnson, K. P., Vartanian, A. M., Jacob, L. M., Lohse, S. E., Torelli, M. D., Hamers, R. J., Murphy, C. J., and Haynes, C. L. (2015) Impacts of gold nanoparticle charge and ligand type on surface binding and toxicity to Gramnegative and Gram-positive bacteria. *Chem. Sci.* 6, 5186–5196.
- (69) Dominguez, G., Lohse, S., Torelli, M., Murphy, C., Hamers, R., Orr, G., and Klaper, R. (2015) Effects of charge and surface ligand properties of nanoparticles on oxidative stress and gene expression within the gut of Daphnia magna. *Aquat. Toxicol.* 162, 1–9.
- (70) Qiu, T. A., Bozich, J. S., Lohse, S. E., Vartanian, A. M., Jacob, L. M., Meyer, B. M., Gunsolus, I. L., Niemuth, N. J., Murphy, C. J., Haynes, C. L., and Klaper, R. D. (2015) Gene expression as an indicator of the molecular response and toxicity in the bacterium Shewanella oneidensis and the water flea Daphnia magna exposed to functionalized gold nanoparticles. *Environ. Sci. Nano 2*, 615–629.
- (71) Falagan-Lotsch, P., Grzincic, E., and Murphy, C. (2016) One low-dose exposure of gold nanoparticles induces long-term changes in human cells. *Proc. Natl. Acad. Sci. 113*, 13318–13323.
- (72) Monopoli, M. P., Aberg, C., Salvati, A., and Dawson, K. A. (2012) Biomolecular coronas provide the biological identity of nanosized materials. *Nat. Nanotechnol.* 7, 779–86.
- (73) Albanese, A., Walkey, C. D., Olsen, J. B., Guo, H., Emili, A., and Chan, W. C. W. (2014) Secreted Biomolecules Alter the Biological Identity and Cellular Interactions of Nanoparticles. *ACS Nano* 8, 5515–5526.
- (74) Gorbenko, G. P. (1999) Structure of cytochrome c complexes with phospholipids as revealed by resonance energy transfer. *Biochim. Biophys. Acta Biomembr. 1420*, 1–13.
- (75) Sweeney, S. F., Woehrle, G. H., and Hutchison, J. E. (2006) Rapid purification and size separation of gold nanoparticles via diafiltration. *J. Am. Chem. Soc. 128*, 3190–3197.
- (76) Brust, M., Walker, M., Bethell, D., Schiffrin, D. J., and Whyman, R. (1994) Synthesis of Thiolderivatised Gold Nanoparticles in a Two-phase Liquid-Liquid System. *J. Chem. Soc. Chem. Commun.* 801–802.
- (77) Li, Y., Zaluzhna, O., Zangmeister, C. D., Allison, T. C., and Tong, Y. J. (2012) Different Mechanisms Govern the Two-Phase Brust Schiffrin Dialkylditelluride Syntheses of Ag and Au Nanoparticles. *J. Am. Chem. Soc. 134*, 1990–1992.
- (78) Orendorff, C. J., and Murphy, C. J. (2006) Quantitation of Metal Content in the Silver-Assisted Growth of Gold Nanorods. *J. Phys. Chem. B* 110, 3990–3994.
- (79) Rodahl, M., Höök, F., Krozer, A., Brzezinski, P., and Kasemo, B. (1995) Quartz crystal microbalance setup for frequency and Q-factor measurements in gaseous and liquid environments. *Rev. Sci. Instrum.* 66, 3924–3930.
- (80) Kedem, O., Vaskevich, A., and Rubinstein, I. (2014) Critical issues in localized plasmon sensing. *J. Phys. Chem. C* 118, 8227–8244.
- (81) Ferhan, A. R., Jackman, J. A., and Cho, N.-J. (2016) Integration of Quartz Crystal Microbalance-Dissipation and Reflection-Mode Localized Surface Plasmon Resonance Sensors for Biomacromolecular Interaction Analysis. *Anal. Chem.* 88, 12524–12531.
- (82) Jonsson, M. P., Jönsson, P., and Höök, F. (2008) Simultaneous nanoplasmonic and quartz crystal microbalance sensing: Analysis of biomolecular conformational changes and quantification of the bound molecular mass. *Anal. Chem.* 80, 7988–7995.
- (83) De Feijter, J. A., Benjamins, J., and Veer, F. A. (1978) Ellipsometry as a tool to study the adsorption behavior of synthetic and biopolymers at the air—water interface. *Biopolymers* 17, 1759–1772.
- (84) Hernandez, R., and Popov, A. V. (2014) Molecular dynamics out of equilibrium: mechanics and measurables. *Wiley Interdiscip. Rev. Comput. Mol. Sci. 4*, 541–561.
- (85) Jo, S., Kim, T., and Im, W. (2007) Automated builder and database of protein/membrane complexes for molecular dynamics simulations. *PLoS One* 2, 1–9.
- (86) Jo, S., Lim, J. B., Klauda, J. B., and Im, W. (2009) CHARMM-GUI membrane builder for mixed bilayers and its application to yeast membranes. *Biophys. J.* 97, 50–58.
- (87) Kyriakou, P. K., Ekblad, B., Kristiansen, E., and Kaznessis, Y. N. (2016) Interactions of a class IIb bacteriocin with a model lipid bilayer, investigated through molecular dynamics simulations. *BBA* -

Biomembr. 1858, 824-835.

- (88) Ardail, D., Privat, J.-P., Egret-Charlier, M., Levrat, C., Lerne, F., and Louisot, P. (1990) Mitochondrial Contact Sites. *J. Biol. Chem.* 265, 18797–18802.
- (89) Humphrey, W., Dalke, A., and Schulten, K. (1996) VMD: Visual Molecular Dynamics. *J. Mol. Graph.* 14, 33–38.
- (90) Jorgensen, W. L., Chandrasekhar, J., Madura, J. D., Impey, R. W., and Klein, M. L. (1983) Comparison of simple potential functions for simulating liquid water. *J. Chem. Phys.* 79, 926–935.
- (91) Nelson, M. T., Humphrey, W., Gursoy, A., Dalke, A., Kalé, L. V, Skeel, R. D., and Schulten, K. (1996) NAMD: a Parallel, Object-Oriented Molecular Dynamics Program. *Int. J. High Perform. Comput. Appl.* 10, 251–268.
- (92) Best, R. B., Zhu, X., Shim, J., Lopes, P. E. M., Mittal, J., Feig, M., and MacKerell Jr., A. D. (2012) Optimization of the Additive CHARMM All-Atom Protein Force Field Targeting Improved Sampling of the Backbone ϕ , ψ and Side-Chain χ 1 and χ 2 Dihedral Angles. *J. Chem. Theory Comput.* 8, 3257–3273. (93) Guvench, O., Mallajosyula, S. S., Raman, E. P., Hatcher, E., Vanommeslaeghe, K., Foster, T. J.,
- Jamison, F. W., Jamison II, F. W., and MacKerell Jr., A. D. (2011) CHARMM additive all-atom force field for carbohydrate derivatives and its utility in polysaccharide and carbohydrate-protein modeling. *J. Chem. Theory Comput.* 7, 3162–3180.
- (94) Klauda, J. B., Venable, R. M., Freites, J. A., O'Connor, J. W., Tobias, D. J., Mondragon-Ramirez, C., Vorobyov, I., MacKerell Jr., A. D., and Pastor, R. W. (2010) Update of the CHARMM All-Atom Additive Force Field for Lipids: Validation on Six Lipid Types. *J. Phys. Chem. B* 114, 7830–7843. (95) Mallajosyula, S. S., Guvench, O., Hatcher, E., and MacKerell Jr., A. D. (2012) CHARMM additive all-atom force field for phosphate and sulfate linked to carbohydrates. *J. Chem. Theory Comput.* 8, 759–776.
- (96) Feller, S. E., Zhang, Y., Pastorbernard, R. W., Brooks, R., Pastor, R. W., and Brooks, B. R. (1995) Constant pressure molecular dynamics simulation: The Langevin piston method. *J. Chem. Phys.* 103, 4613–4621.
- (97) Darden, T., York, D., and Pedersen, L. (1993) Particle mesh Ewald: An N·log(N method for Ewald sums in large systems. *J. Chem. Phys.* 98, 10089–10092.
- (98) Castagnola, V., Zhao, W., Boselli, L., Lo Giudice, M. C., Meder, F., Polo, E., Paton, K. R., Backes, C., Coleman, J. N., and Dawson, K. A. (2018) Biological recognition of graphene nanoflakes. *Nature Commun.* 9, 1-9.

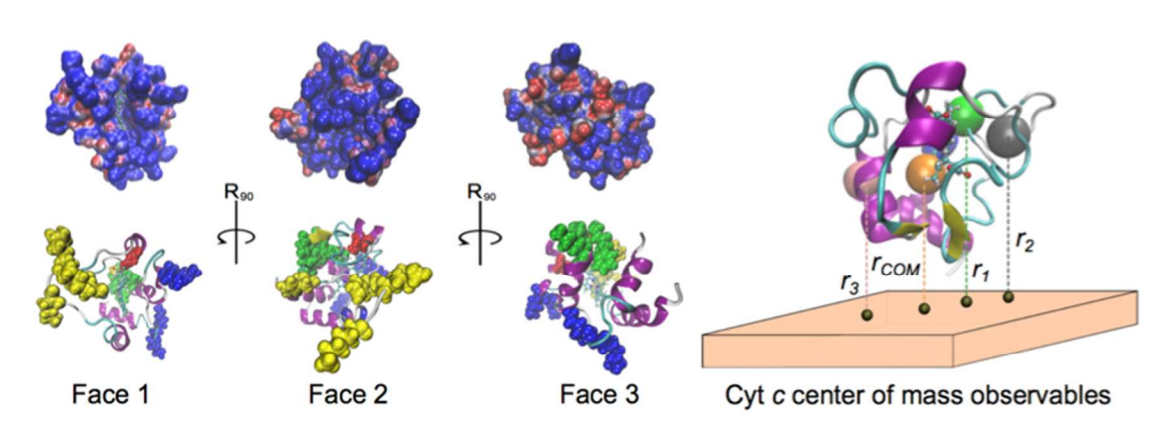


Figure 1. Cytochrome c (cyt c) structure. Three adaptive Poisson-Boltzmann electrostatic surface area maps are shown (top left) for the protein in orientations such that the corresponding face directed toward the lipid bilayer surface in the MD simulations faces the reader. Blue indicates regions of positive charge, red indicates negative charge, and white indicates neutral regions. Face 1 (left) shows the mostly electropositive face of cyt c, face 2 (middle) is a 90° rotation from the electropositive face, and face 3 (right) shows a further 90° rotation from face 2. Below each of these images, a van der Waals space-filling representation in the same orientation is shown to highlight the putative cardiolipin binding sites: site A in blue, site L in yellow, site N in green, and site C in red. The four center of mass (COM) distances defined from the closest point on the surface of the bilayer to each of the three selected faces of cyt c and the entire protein are illustrated at right: r_{COM} is the distance between the COM of cyt c and the bilayer surface, r_1 is the distance from the COM of face 1 (green) to the bilayer surface, r_2 is the distance from the COM of face 2 (grey) to the bilayer surface, and r_3 is the distance from the COM of face 3 (pink) to the bilayer surface.

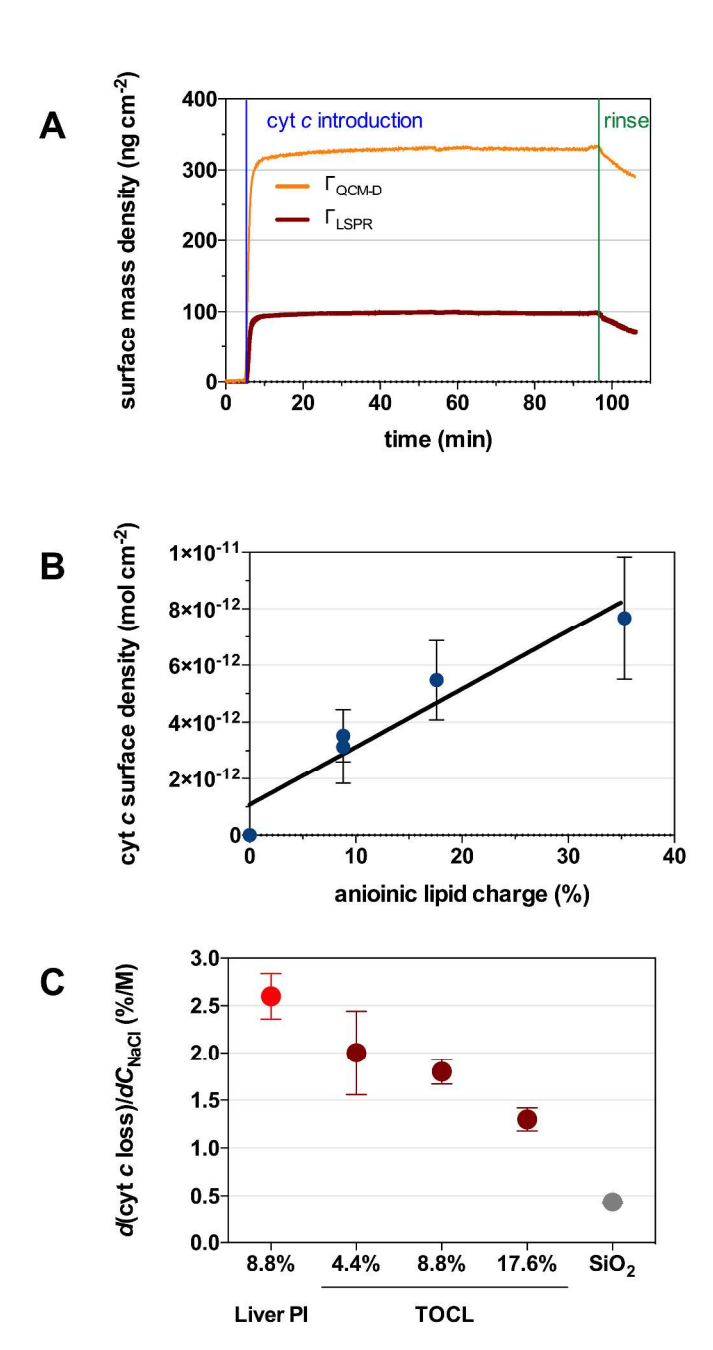


Figure 2. Cytochrome c (cyt c) incorporation into and release from DOPC bilayers containing the TOCL or Liver PI. (A) Acoustic and optical mass densities for cyt c association with a DOPC bilayer containing 17.6 mol% cardiolipin derived respectively from QCM-D data (orange line) using the Sauerbrey equation (Eq 1) and localized surface plasmon resonance (LSPR) data (maroon line) using the de Feijter formula (Eq 2). Cytochrome c was delivered at 50 mg·L⁻¹ in 0.01 M NaCl buffered to pH 7.4 with 0.01 M HEPES. The QCM-D and LSPR traces are presented in Figure S3. (B) Surface density of cyt c molecules as a function of anionic lipid charge in model membranes. Error bars indicate one standard deviation of triplicate measurements. Numerical values provided in Table S2. (C) Ionic strength-induced dissociation of cyt c from supported DOPC bilayers containing the indicated amount of anionic phospholipid

(mol %) or from silica surfaces. Numerical values provided in Table S4. Error bars indicate the standard deviation of triplicate measurements.

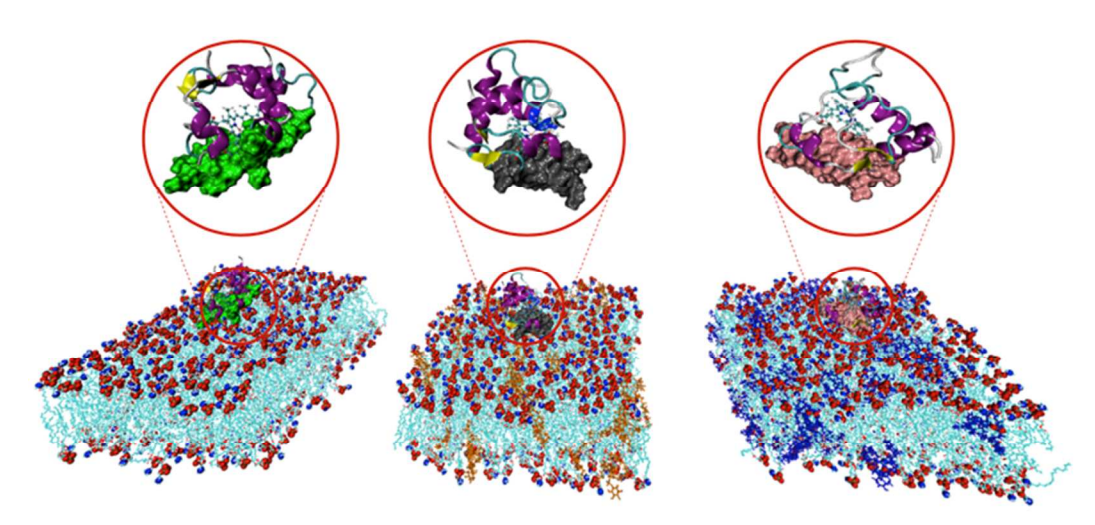


Figure 3. The three bilayers (left to right: 100% DOPC, 9:1 DOPC:SAPI, and 9:1 DOPC:TOCL) considered in this study are shown with the three respective faces – highlighted in Figure 1 – of cyt c physisorbed onto the surface. The amino acids that compose each cyt c face (1, 2, and 3) are shown in green, grey, and pink, respectively. The acyl chains of the DOPC lipids are shown in cyan, those of SAPI are in orange, and those of TOCL are in blue. van der Waals spheres of the nitrogen atoms of the DOPC choline head groups are shown in blue, and the DOPC phosphate oxygen atoms are shown in red. TIP3P water molecules and salt ions are omitted for clarity. Above each lipid bilayer system, cyt c is scaled to enhance the view of the oriented structure.

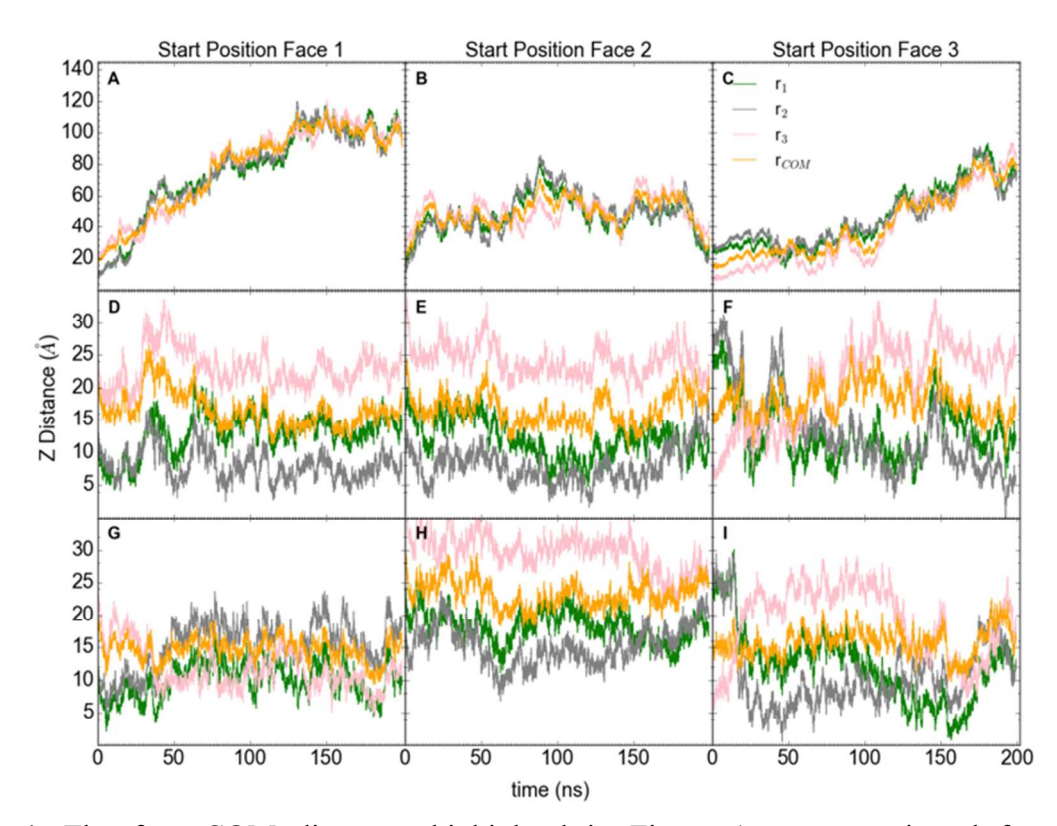
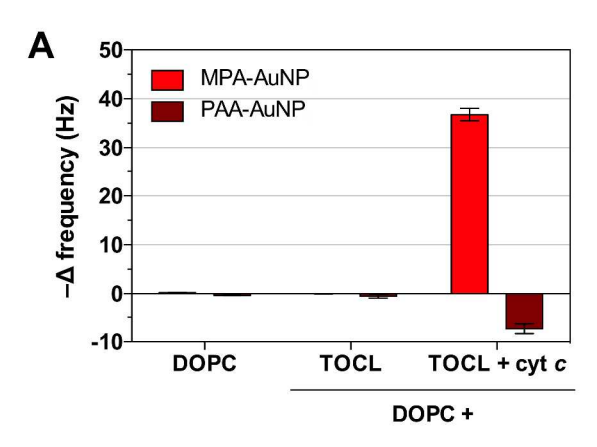
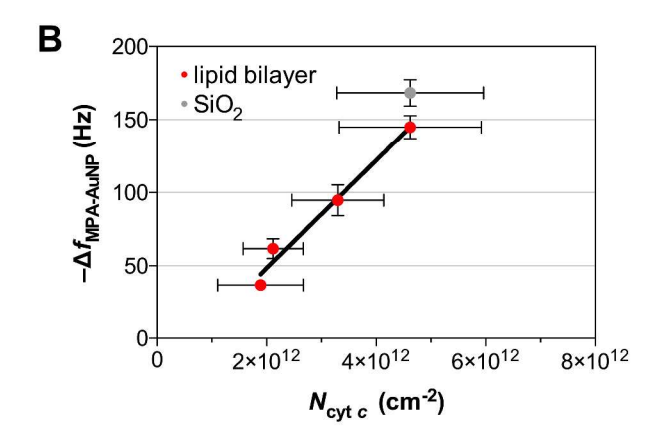


Figure 4. The four COM distances highlighted in Figure 1 were monitored for all nine trajectories. The green, grey, pink, and goldenrod curves are the measured distances between the bilayer and the COM of face 1 (r_1) , face 2 (r_2) , face 3 (r_3) or the cyt c molecules (r_{COM}) , respectively. Panels A-C are for the 100% DOPC bilayer; panels D-F are for the 9:1 DOPC:SAPI bilayer; and panels G-I are for the 9:1 DOPC:TOCL bilayer.





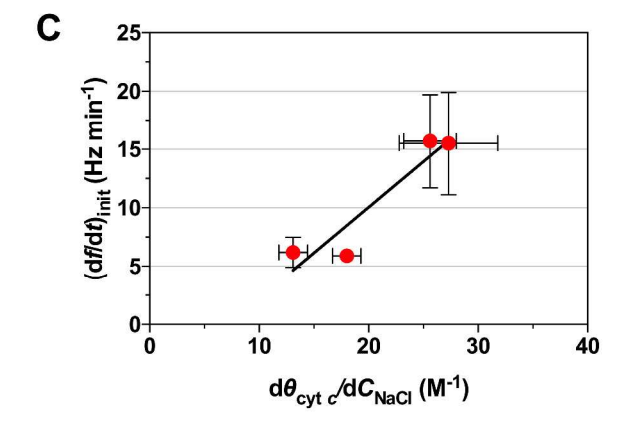


Figure 5. The presence of cytochrome c on the membrane surface alters nanoparticle interaction with model biological membranes. (A) Representative data of MPA- and PAA-AuNP interaction with supported lipid bilayers. The TOCL content of cardiolipin-containing bilayers was 4.4 mol%. Changes in frequency are expressed relative to the (cyt c-containing) supported lipid bilayers prior to introduction of nanoparticles. Error bars indicate one standard deviation of triplicate measurements. Data for supported DOPC bilayers with higher TOCL contents are presented in Table S7. (B) Attachment of MPA-AuNPs to supported lipid bilayers with bound cyt c correlates strongly with the amount of cyt c bound to the bilayer ($-\Delta f_{\text{MPA-AuNP}} = (3.7 \times 10^{-4})$).

 10^{11})· $N_{\rm cyt\ c}$ – 25, where $N_{\rm cyt\ c}$ is the number density of cytochrome c molecules; p=0.0106, $R^2=0.978$) and differs from cyt c bound to silica. In (B), vertical and horizontal error bars indicate the standard deviation of MPA-AuNP attachment and number density of cyt c molecules of triplicate measurements, respectively. Surface number densities of cyt c associated with Liver PI-and TOCL-containing bilayers presented in Table S9. (C) The rate of apparent cyt c removal by PAA-AuNPs from supported lipid bilayers ((df/dt)_{init})) correlated strongly with the "strength" of cyt c binding (p=0.0608, $R^2=0.882$) as determined by the change in fractional coverage of cyt c ($\theta_{\rm cyt\ }c$) per unit change in NaCl concentration ($d\theta_{\rm cyt\ }c/dC_{\rm NaCl}$). In (C), vertical and horizontal error bars indicate one standard deviation from triplicate measurements in the release rate and the slope of the cyt c release curve, respectively.

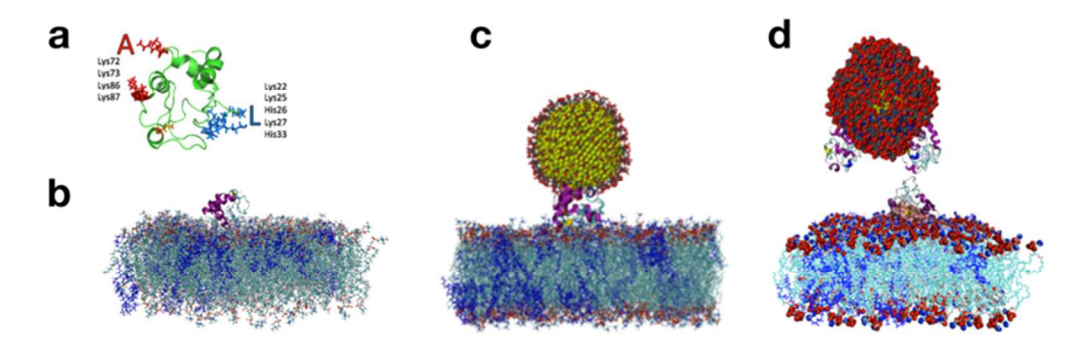


Figure 6. The peripheral membrane protein cytochrome c (cyt c) mediates the interaction of anionic gold nanoparticles with phospholipid bilayers. (A) Ribbon diagram of cyt c highlighting basic amino acid residues in sites A and L. (B) Cytochrome c bound via site A to a phospholipid bilayer composed of zwitterionic DOPC and anionic TOCL was not seen in the case of SAPI (which bound primarily to face 2). We note that a subpopulation of cyt c binds with site L oriented towards the membrane. (C) Anionic MPA-AuNPs attachment to model membranes illustrates the hypothesis of mediated binding to cytochrome c via site L. (D) Anionic PAA-AuNPs binding to cyt c via site L and removing the protein from the membrane under this hypothesis.

